Available online at www.sciencedirect.com
SCIENCE DIRECT
Polymer 46 (2005) 4454–4464
polymer
www.elsevier.com/locate/polymer

Reaction induced phase-separation controlled by molecular topology

Amit S. Kulkarni, Gregory Beaucage*

Department of Chemical and Materials Engineering, University of Cincinnati, Cincinnati, OH 45221-0012, USA

Available online 8 March 2005

Abstract

Binary phase-separation driven by a difference in branch content of the two components has been widely reported in polyolefins. This concept is applied to polysiloxanes in an attempt to control morphology in chemically driven phase separation. It is shown that self-assembled, non-reversible spinodal morphologies (SD) as well as low-polydispersity nucleation and growth morphologies can be controlled through the rate of network formation in these systems. Time-resolved light scattering and optical microscopy were used to determine the character and kinetics of phase separation. The mechanism of phase separation in two similar systems was dictated by the rates of the crosslinking reactions. Both morphologies were 'locked-in' by network formation and late-stage phase-ripening was prevented by low surface energy associated with topologically driven phase-separation.

Keywords: Phase separation; PDMS networks; Branching

1. Introduction

Bimodal network's, formed by crosslinking end-functionalized chains of high molecular-weight with low molecular-weight or oligomeric chains have been shown to improve toughness and tear resistance [1,2], compared to monodisperse networks. Phase-separation in such networks has been largely avoided [3]. In this article, bimodal networks are used to study the effect of chain topology on phase-separation.

The effect of crosslinking on the phase-separation behavior has been well documented by various authors over the years [4–7]. Crosslinking brings about an increase in the molecular weights of the components as well as change in chain entropy and free energy. This could drive the system from an initially homogenous, one-phase region, to a two-phase region [8].

Some literature reports indicate that phase-separation can be obtained in multimodal networks during network formation [9]. For example, in a bimodal poly(dimethyl siloxane), PDMS, network formed via hydrosilation of vinyl end-functionalized precursors, formation of spinodal-like structure is reported [10]. The structure differs from a true spinodal since it is non-reversible [11,12]. This observation is in agreement with the works of Schulz and Paul [13] and Kita et al. [14], which showed that crosslinking induced phase-separation in networks leads to the formation of a morphology, which is 'locked-in', and late stage decomposition to polydisperse non-correlated domains is not seen.

The phase-separation phenomenon in gelling systems is reminiscent of network-modified miscibility suggested by deGennes a number of years ago [15,16]. It is proposed, following deGennes, that network formation and phase-separation are collaborative events at an early stage, under these conditions, and the process represents a balance between thermodynamic and kinetic interests.

In our bimodal networks, phase-separation does not involve a conventional mixture of chemically different species, but involves a blend where the two phases differ, for the most part, topologically, that is in terms of branch content or crosslink density. Wignall et al. [17] have shown that phase separation can be triggered by differences in the topology of the two phases in blends of polyolefins. They have investigated blends of linear high-density polyethylene (HDPE) and linear low-density polyethylene (LLDPE), which has a high content of short-chain branching. It is possible that such topologically driven phase-separation can be generalized to other branched systems such as polysilioxanes.

* Corresponding author. Tel.: +1 513 556 3063; fax: +1 513 556 3773.
E-mail address: beaucag@uc.edu (G. Beaucage).

0032-3861/$ - see front matter © 2005 Elsevier Ltd. All rights reserved.
doi:10.1016/j.polymer.2005.02.028

2. Experimental

2.1. Synthesis

Two bimodal network systems were studied that varied in conversion time profile; a vinyl-terminated, rapid conversion system and a sol–gel system with much slower conversion and a lower final conversion.

2.1.1. Vinyl-terminated system

All the chemicals for the vinyl-terminated system were purchased form Gelest Inc. Two different molecular weight pre-polymers were used to form the networks. For the vinyl system, the low molecular weight oligomeric material used was 1, 3-divinyl tetramethyl-disiloxane of molecular weight 186.4 g/mol. The high molecular weight pre-polymer used was vinyl-terminated polydimethylsiloxane (PDMS) (22,000 g/mol). The crosslinker was tetrakis(dimethylsiloxy)-silane and the catalyst used was platinum-divinyl tetramethyl disiloxane complex in xylene, also known as Karstedt's catalyst [18]. The catalyst was used to catalyze the end-linking reaction. The product of this reaction is H_2 gas which solubalizes in the polymer/oligomer mixture and is quickly outgassed to the environment with no observable bubbles.

2.1.2. Hydroxyl-terminated system

In the silanol terminated system, the pre-polymers used were silanol-terminated PDMS of molecular weights 750 and 18,000 g/mol obtained from Gelest Inc. Tetraethylorthosilicate (TEOS) of 98% purity from Aldrich was used as the crosslinker. Dibutyl tin dilaurate, 25% in cyclic dimethyl siloxane from United Chemicals Technologies Inc. was used as the catalyst. The hydrolysis/condensation reaction [19] results in the formation of four ethanol molecules per TEOS in the hydrolysis reaction, consuming four water molecules followed by the release of two water molecules per molecule of TEOS on condensation. The total hydrolysis/condensation reaction consumes 2 mol of water and produces 4 mol of ethanol per mole of TEOS while the end-linking reaction does not consume water. Ethanol is generally outgased and or extracted from the final network. For our in situ studies, forced outgassing using a vacuum was not possible leading to an even slower rate of gelation and network formation. The rate of increase in molecular weight was lower in the hydroxyl system as compared to the vinyl system as evident from a much longer gelation time.

For chemically-driven phase-separation the extent of reaction parallels the thermal quench-depth in traditional thermally controlled phase-separation. In this context, the hydrosilation system represents a deep quench condition, far from the critical point, while the hydrolysis/condensation system represents a shallow quench condition near the phase-separation boundary.

2.2. Network formation

2.2.1. Vinyl-terminated system

Vinyl-terminated, bimodal networks were formed using 98–99.5 mol% of short chains and the remainder long chains. This represents roughly a 50% mixture by volume. A stoichiometric amount of crosslinker was employed in all the formulations.

Catalyst loading appears to be vital to production of the spinodal-like structure in the vinyl system, presumably due to the influence of the rate of crosslinking on the development of the spinodal-like morphology. It was found that the minimum amount of catalyst for gelation and network formation was optimal and in order to achieve relatively low catalyst concentrations the initial catalyst solution was diluted in toluene to 10% by volume of the initial solution. Through trial and error it was found that 0.5 mg of this diluted catalyst per gram of base polymer mixture was optimal for production of the spinodal-like structure. Networks produced under these conditions showed phase-separation in bulk when synthesized in a glass vial as well as when synthesized between glass cover slips. It should be noted that thin films prepared by placing a drop of the reaction mixture on a single glass cover slip, open to the atmosphere, did not display phase-separation. This may be associated with the sensitivity of the hydrosilation reaction to atmospheric oxygen.

2.2.2. Hydroxyl-terminated system

The hydrolysis/condensation system consisted of 98.5 mol% short chains (about 50% by volume) and also utilized a stoichiometric amount of tetraethylorthosilicate, TEOS, crosslinker. Dibutyl tin dilaurate catalyst loading was varied from 2–5% by weight of the polymer mixture. Samples were prepared on microscope cover slips, both open to atmosphere and sandwiched. Water, required for hydrolysis, was provided by ambient H_2O. For the hydroxyl-terminated system no difference in phase-separation was observed between open and closed films.

2.3. Light scattering measurements

Light scattering (LS) was performed on samples prepared between glass cover-slips with a sample thickness of about 1 mm. A 20 mW helium–neon gas laser at 632.8 nm wavelength was used. Using a single pinhole near the sample, the scattering pattern was projected on a screen and imaged with a CCD camera, Princeton Instruments Optical Multichannel Analysizer (OMA) [20–23]. Background scattering from an identical sample except for the absence of crosslinker was subtracted from the light-scattering patterns. The data was corrected for $1/r^2$ decay due to the flat projection of the scattering pattern; and the isotropic 2D data was radially averaged. A schematic of the light scattering setup is shown in Fig. 1.

In order to determine possible differences in the chemical

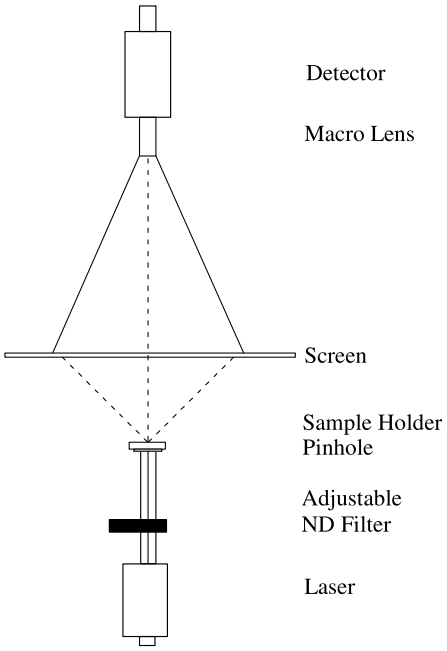

Fig. 1. Light scattering experimental set-up to study phase separation and gelation kinetics.

composition of the phase-separated systems IR measurements were performed. Attenuated, total-reflectance IR spectra of the samples were measured using a Nicolet Magna 760 infra-red spectrometer. The spectra were obtained by summing 256 scans on the samples.

Optical micrographs of the same samples were obtained using a Nikon Optiphot2-pol optical microscope connected to a PC. The digital images were obtained using Image Pro 4.1 software.

3. Results and discussion

3.1. Vinyl-terminated system

For the hydrosilation system, the onset of spinodal-like decomposition, as measured by time resolved LS, took place approximately at the gel point, which was at about 20 min after mixing. It took about 45 min for significant turbidity to be observed in the bulk state. As noted above, spinodal-like decomposition is absent from samples produced as open slides. This indicates that atmospheric oxygen, water, or transport of evaporating components might interfere with the crosslinking reaction. The correlation-ring pattern in light scattering, Fig. 2 inset, is a hallmark of spinodal decomposition. The ring indicates the formation of a correlated structure with no preferred orientation. The structure formed has co-continuous morphology as seen in optical micrographs, Fig. 2.

Fig. 3 shows radially averaged, azimuthal, time-resolved light-scattering plots of intensity versus the scattering vector $q=4\pi \sin(\theta/2)/\lambda$, following the progress of the spinodal-like decomposition, where λ is the wavelength and θ is the scattering angle. As in conventional spinodal decomposition, we see an increase in the intensity of the peak with time. The peak obtained in these plots is due to correlation between phases, with the angle of maximum intensity, q^*, corresponding to the correlation distance $\xi=2\pi/q^*\sim 2.2$ μm.

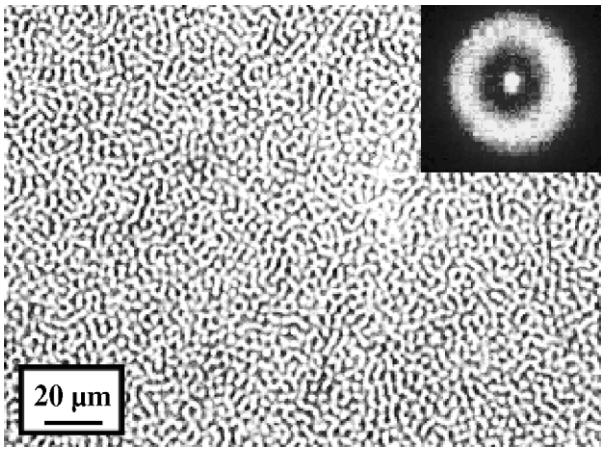

Fig. 2. Phase-separated, co-continuous structure related to spinodal-like decomposition in the hydrosilation system. The spinodal-like, correlation distance is approximately, 2.2 microns both in the micrograph and in the SALS pattern, inset, as discussed in the text.

Normally, for linear polymer mixtures at deep thermal quenches, a spinodal-peak is seen to decay to lower-q and to broaden as Ostwald ripening occurs at later stages of phase separation driven by the reduction in free energy of the system through reduction in the surface area of phases [22–24]. Surprisingly, in the crosslinked system, phases are not observed to ripen whatsoever (Fig. 3). We attribute this to the presence of a gel structure, which limits transport as well as, possibly, a limited surface-energy difference between phases of similar chemical composition differing mainly in crosslink density. That is, ripening might not be expected if the surfaces of the two phases are chemically similar since size growth is driven by a reduction in surface area to minimize the free energy. The end effect is that the early-stage spinodal-like structure is 'locked-in' [13,14] and a permanent early-stage spinodal-like structure results (Fig. 2).

Attenuated total reflectance infra-red (ATR-IR) spectra of two samples, a bimodal sample having undergone spinodal-like decomposition and the second of a normal mono-modal PDMS network formed from vinyl end-linked precursors is shown in Fig. 4. Comparison of the two spectra fails to show a chemical difference between the phase-separated sample and the normal mono-modal PDMS network. This indicates that the phase-separated domains may not arise due to differences in chemical composition.

Wignall et al. [17] have demonstrated the occurrence of phase-separation in blends of linear and branched polyethylene's arising from a disparity in branch content

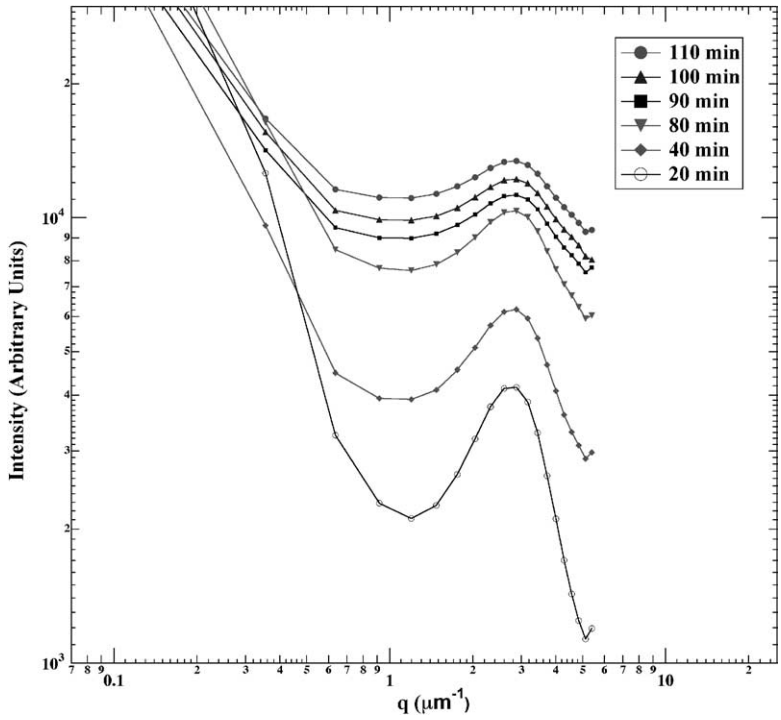

Fig. 3. Time-resolved, light-scattering plot. Log-scattered intensity versus log-q. The peak position indicates correlated domains at 2.2 micron spacing in agreement with Fig. 2. Ripening of the phase-structure at late stage is not observed, i.e. the peak position remains constant at late stages of decomposition.

amongst the separated phases. Their work, in addition to previous literature [25–27], indicates that blends whose constituents are of similar chemical species but are topologically different can undergo phase separation. The work of Alamo et al. [28] quantified the critical amount of branching in a blend of linear and branched polyethylene which would lead to phase separation. They found this critical value of branch content to be $\geqslant 8$ branches/100 backbone carbon atoms of the branched constituent. In order to derive an analogue for our system it is assumed that the high-molecular-weight precursor forms a phase dominated by linear chains. The low molecular weight PDMS chains are found to have ~ 28 branches/100 backbone atoms for the vinyl-terminated system, and ~ 10 branches/100 backbone atoms in the hydroxyl-terminated system. So it is possible for the observed phase-separation in our system to arise from topological differences in the phases if Alamo's results can be generalized to other topological systems.

A schematic of the difference in the kinetic nature of the reactions taking place in the vinyl and hydroxyl-terminated systems is shown in Fig. 5. The vinyl-terminated system undergoes crosslinking by an addition mechanism. It is

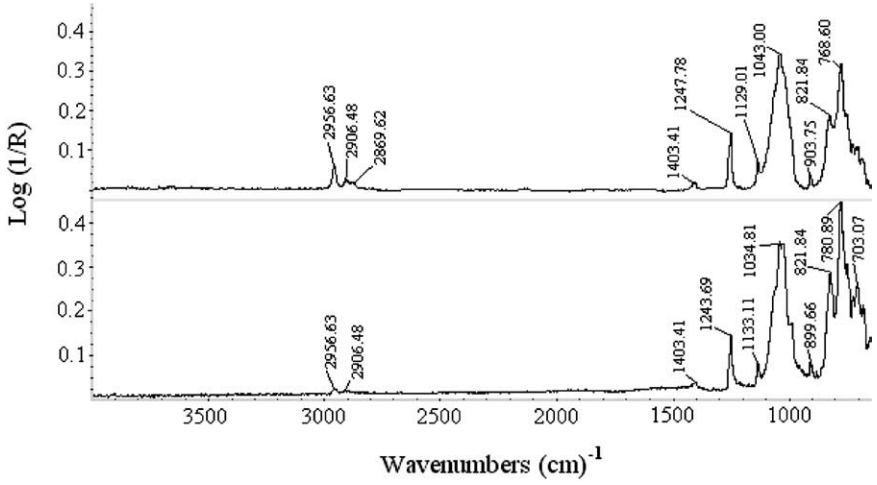

Fig. 4. ATR-IR Spectra, Top: Bimodal (186.4: 22,000 g/mol) PDMS network showing spinodal-like phase-separation, Bottom: Monomodal PDMS network formed from vinyl end-linked chains of 22,000 g/mol.

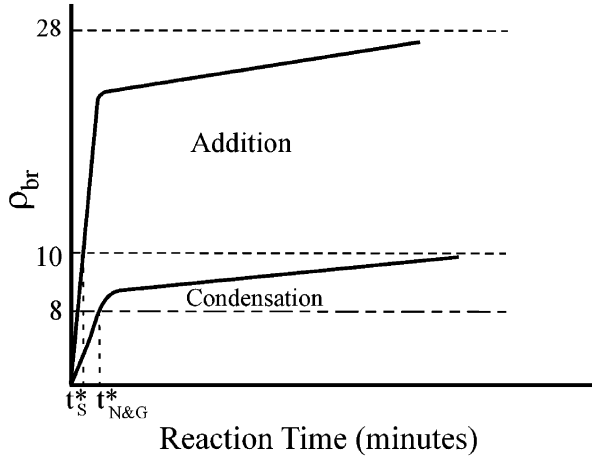

Fig. 5. ρ_{br} versus Reaction time where ρ_{br} = number of branches/100 backbone atoms. Schematic of proposed reaction kinetics in the vinyl (addition) and hydroxyl (condensation) terminated systems. t^*_S is the time for onset of spinodal-like phase separation in the vinyl system. $t^*_{N\&G}$ is the time for onset of nucleation and growth in the hydroxyl system. The value of 8/100 is from reference [28]. Ten and 28 are calculated values described in the text.

proposed that due to the relatively fast nature of this reaction [29], the system is rapidly quenched into the two-phase region demarcated by the critical branch content of 8/100 in Fig. 5 (ordinate). Moreover, since it is possible for the addition reaction to go to completion [29], the quench obtained is not only fast but deep as well, i.e. far from the phase-separation boundary; lower dashed line in Fig. 5 as generalized from Alamo [28].

On the contrary, in the hydroxyl-terminated system, discussed in the next section, a condensation reaction is responsible for crosslinking. The reaction rate of such a condensation reaction [29] can be maintained only if the condensation product; ethanol in our case, is continuously removed from the system. As this is not possible for the in situ measurements, the quench obtained in the hydroxyl-terminated system is much shallower as compared to the vinyl-terminated system. This may lead to a different mechanism of phase separation in the hydroxyl-terminated system as will be discussed below.

Fig. 6 shows a schematic mechanism that explains a possible progression for the crosslinking reaction and the subsequent formation of separated phases for both vinyl and hydroxyl-terminated systems. The different stages can be explained as follows: (a) short and long chains are mixed before initiation of reaction. (b) On addition of a tetra-functional crosslinker, short chains react more rapidly due to their higher density of reactive sites and higher mobility, which allows diffusion towards reaction sites. (c) The short chains react further from their terminal reactive sites; reaction of both end groups of the short chains leads to chain extension, the onset of phase separation and gelation may be near this schematic stage. The arrows in Fig. 6(c) indicate transport due to topological immiscibility. (d) Chain extension decreases the difference in size of the precursor short and long chains, the short and long chains now have similar probabilities of diffusing to the reaction sites, (e) 'locking-in' of two phases rich in highly branched short chains and relatively linear long chains.

3.1.1. Contrast

The contrast between the phases for light scattering experiments could possibly arise due to the difference in density of the separated phases associated solely with the crosslink density difference. One of the phases is rich in crosslinked, short precursor chains (Fig. 6(e)), whereas, the other phase comprises mostly long linear chains reacted only at the ends. The density difference can be estimated by the method of group contribution suggested by Bondi [30,31]. Using this method $\Delta\rho$ was calculated to be 0.06 g/cm^3 for the vinyl-terminated system and 0.02 g/cm^3 for the hydroxyl-terminated system. The higher density difference in the vinyl-terminated system is partially due to shorter short chains as well as the presence of (–CH_2–CH_2–) groups in the short chains, which remain embedded in the system due to the addition reaction mechanism. These groups could also further drive the deep quench for the vinyl-terminated system.

The Lorenz–Lorentz equation [32], gives the relationship between the density and refractive index for spherical molecules as,

$$\frac{n^2-1}{n^2+2} = C\rho \tag{1}$$

where n is the refractive index, ρ is the density and C is a constant known as the specific refraction and is given by the ratio of molecular refraction to the molecular mass. Eq. (1) can be used as an approximation for the crosslinked phases to gain an idea of the feasibility of contrast in the light scattering measurement. The difference in the refractive indices of the two phases when calculated from Eq. (1) is found to be nearly 0.09 for the vinyl-terminated system and 0.02 for the hydroxyl-terminated system, which is a sufficient contrast for scattering of light [33]. Then it is feasible that phase-separation, driven by a large difference in crosslink density between short and long chains could give rise to the observed SALS patterns. The observed dependence on catalyst concentration and crosslinking reaction is consistent with this model.

3.2. Spinodal analysis

The kinetics of the early stage spinodal decomposition can be explained on the basis of the linearized Cahn–Hilliard theory [11,34–36]. According to their theory, concentration fluctuations associated with spinodal decomposition, in the early stages, display a linear rate law, $\delta\varphi \sim (R\varphi)\mathrm{d}t$, where R is the linear growth rate, φ is the concentration and t is the time [37,38]. This corresponds to an exponential increase in the scattered intensity of light on

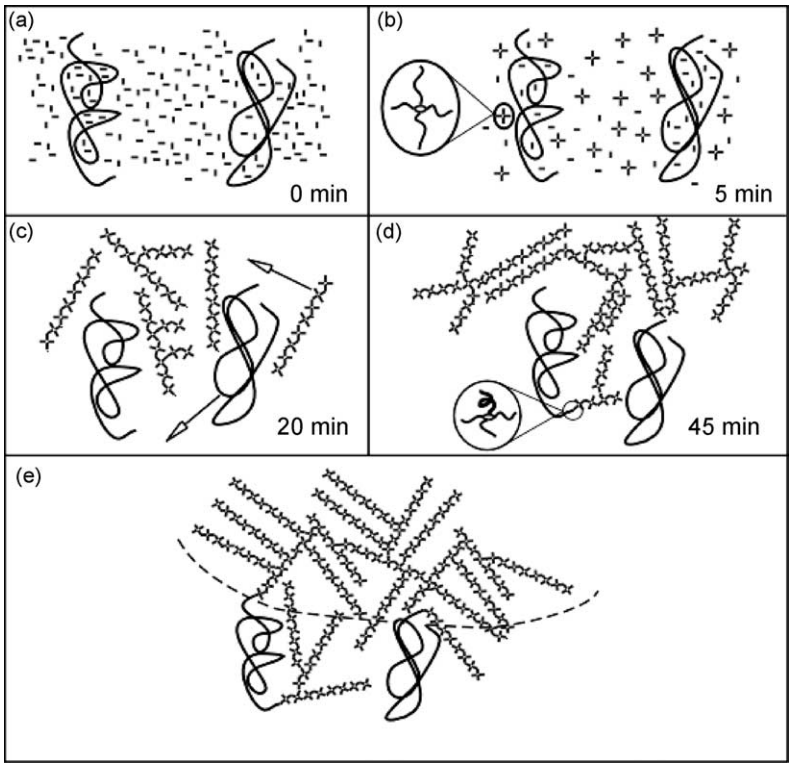

Fig. 6. Schematic of the proposed reaction mechanism leading to phase separation, discussed in the text.

integration, and is given by Eq. (2) as,

$$I(q,t) = I(q,t=0)\exp[2R(q)t] \tag{2}$$

where $I(q,\ t=0)$ is the scattered intensity at zero time associated with native composition fluctuations, and $R(q)$ is the rate of phase separation. From Fig. 3, the maxima in scattered intensity occurs at a wave vector q_m of 2.8 μm^{-1}. This value of maximum scattering vector does not change with time.

The time-evolution of scattered intensity shown in Fig. 3 has an interesting characteristic. The peak obtained in the intensity at wave-vector 2.8 μm^{-1} is because of the spinodal correlation length between the phases, as can be seen in the micrograph (Fig. 2). But, in addition to the growth of this peak, a flat background intensity increases in time and seems to 'wash-out' the spinodal peak at latter stages. This increasing background intensity may be associated with the growth of sub-micron scale clusters of branched chains.

The total scattering obtained in Fig. 3, is then a sum of two contributions, scattering due to the evolution of the spinodal morphology, and scattering arising from growing network clusters. The spinodal scattering at high-q reflects a random 3-D web structure on a micron scale. Scattering from such an interpenetrating fractal structure can be approximated by $I \sim Bq^{-d_f}$. For a random walk structure with intersection of paths, (Brownian walk), $d_f \sim 2$. The total scattered intensity at high-q, above the spinodal peak, could then be given as,

$$I(q) \sim B(t)q^{-2} + C(t) \tag{3}$$

The first term on the right-hand side of Eq. (3) represents the contribution from the random spinodal structure at sizes smaller than the correlation length, i.e. high-q, above the peak position in q. The second term is the contribution from the growing nano-scale clusters, and is a time dependent term, as molecular cluster growth progresses with time. Fits for the high-q scattering data using Eq. (3) are shown in Fig. 7.

Since $C(t)$ represents the low-q Rayleigh limit for nano-scale cluster scattering, it can be expressed as,

$$C(t) \sim N_{cluster}[d_{cluster}(t)]^6 \tag{4}$$

where, $N_{cluster}$ is the number density of growing molecular clusters, and is assumed to be a constant, and $d_{cluster}$ is the size of the branched nanoscale molecular clusters. The molecular clusters are fractal objects with $d_{cluster} \sim z^{1/df}$, where z is the weight average molar mass (number of molecular units) of a cluster and d_f reflects the average mass-fractal dimension of a cluster. We assume $d_f = 2$, as an approximation. Using this approximation, since d_f cannot be measured in the available q-range, we get,

$$C(t) \sim z^3(t)$$

$$\therefore C(t)^{1/3} \sim z(t) \tag{5}$$

In Fig. 8 $\log C(t)^{1/3}$ is plotted against log t to approximate the growth of z in time for the molecular clusters. A power–

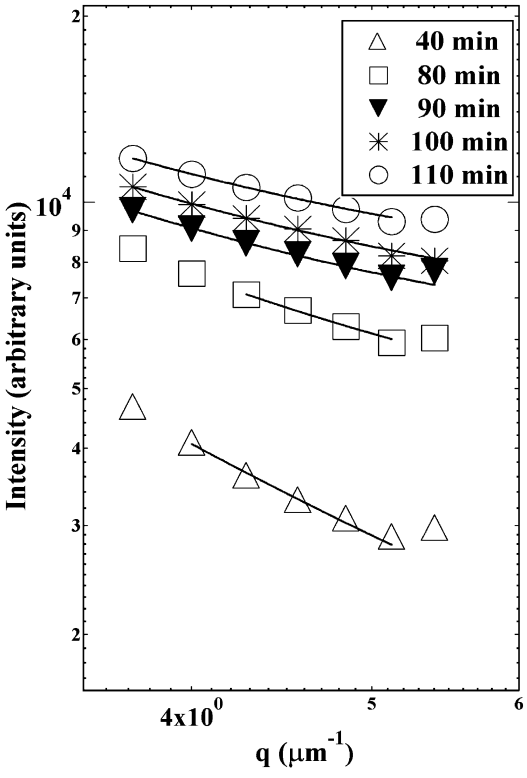

Fig. 7. Log–log plot of intensity versus q, at high-q, showing fits to Eq. (3) used to estimate $C(t)$.

law relationship is observed, approximately, $z \sim t^{1/2}$ (dash-dot line) which reflects a slow growth in molar mass compared with conventional models, diffusion limited growth would indicate $z \sim t$ for instance [39]. Fig. 8 indicates that the plateau for addition polymerization, Fig. 5, is correct, here with a weak $t^{1/2}$ slope, and that the initial, rapid conversion occurs prior to 20 min reaction time in Fig. 8 (solid line).

The intensity data, from Fig. 3, were corrected for this contribution arising from network formation, $C(t)$ in Eq. (3), and plotted against time, as shown in Fig. 9, (following Eq. (2)) which shows a plot of intensity arising from spinodal decomposition at various q-values versus time. The rate of phase-separation, $R(q)$, [40] is calculated form the slopes of Fig. 9 and the projected initial spinodal intensity, $I_{t=0}(q)$, is obtained from the intercept. $I_{t=0}(q)$ reflects a hypothetical initial intensity under constant quench conditions for the reacting system. In the hydrosilation system, the reaction is rapid enough for the approximation of a constant quench depth, Fig. 5 as supported by Figs. 8 and 9. This approximation is better in the latter stages.

Fig. 10 shows the variation in the rate of phase-separation $R(q)$, and the hypothetical extrapolated intensity at zero time $I_{t=0}$, as a function of q. As we can see from the wave-vectors at which a maxima in the values of $R(q)$ and $I_{t=0}$ are observed, the manifestation of the maximum growth rate in the scattering experiment ($I_{t=0}$) occurs at a length scale smaller than the maximum growth rate itself. Normally, phase ripening is observed in spinodal decomposition driven by a reduction in surface area [22–24] leading to an increase in size for q^*. The data shows the opposite of this behavior as $q^* < q_{I_{t=0}}$. This indicates that the phases observed do not have the thermodynamic potential or drive,

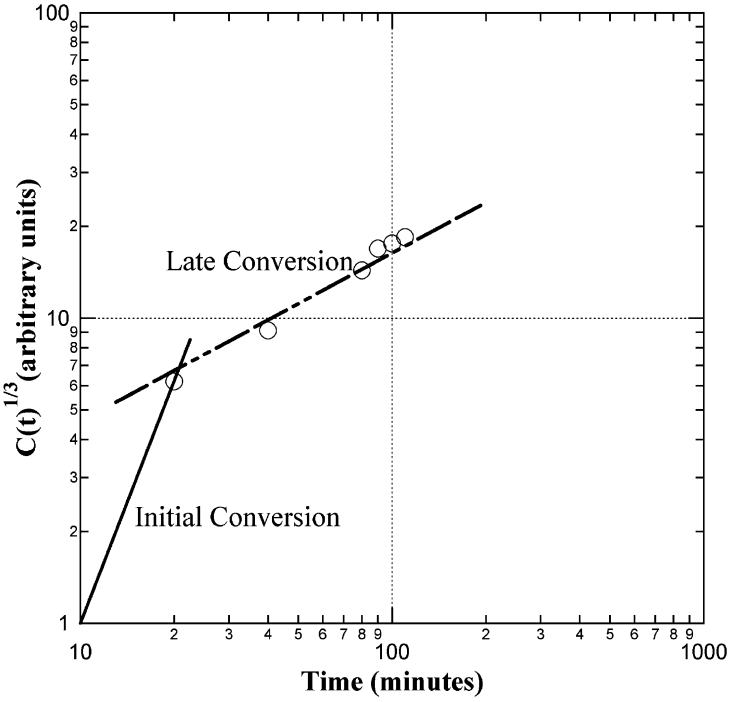

Fig. 8. log–log plot of the cube root of scattered intensity ($C(t)^{1/3}$) arising from network formation versus time, where $z \sim [C(t)]^{1/3}$. Dot-dashed line follows $z \sim t^{1/2}$ as discussed in text.

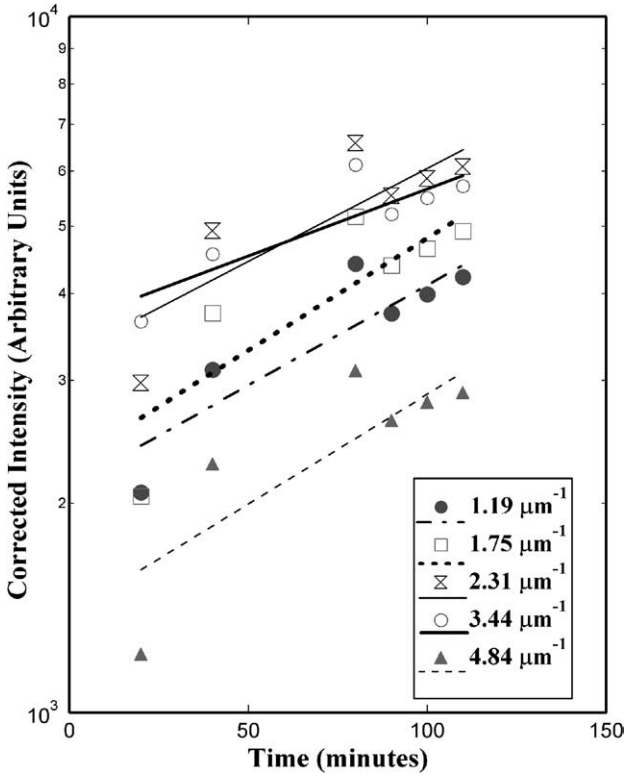

Fig. 9. Log-linear plot of corrected intensity arising from spinodal decomposition, versus time for the vinyl-terminated system.

to ripen at latter stages. The explanation for this could be that the phases, being of similar chemical compositions, with limited surface energy difference, do not need to further reduce their interfacial area. Additionally, the progressive network formation, taking place due to the reaction, could 'squeeze-in' these phases following deGennes [15,16], thus preventing an increase in size.

According to the linear Cahn–Hilliard approximation, it is expected that $R(q)/q^2$ linearly decreases with q^2:

$$R(q) \sim Dq^2\left[\frac{\partial^2 f}{\partial c^2} - \kappa q^2\right] \tag{6}$$

Fig. 11 shows that this approximation is partially met for the hydrosilation system, dashed line. The x-intercept of the dashed line in this plot gives the value q_c, which is the extrapolated critical wave-vector at which there is a crossover [37] from positive to negative values of growth rate $R(q)$, i.e. the stability limit in size, $1/q_c$, for spinodal domains; domains smaller than $\sim 1/q_c$ are not stable. Cahn–Hilliard theory, predicts that $q_c^2 = 2q^{*2}$, or that the phase size for maximum growth, q^*, and the critical phase size are related by $\sqrt{2}$. The data for the hydrosilation system agrees with the classical prediction,

$$2q^{*2} = q_c^2 \tag{7}$$

The value of q_c^2 obtained from Fig. 11 is 10.74, which is in close agreement with the value of $2q^{*2}$ of 10.67, from Fig. 10(a).

The theory of early stage spinodal decomposition, which is based on the linearization approximation, matches the result of Fig. 11. However, the late stage of spinodal decomposition, which is usually characterized by a deviation from linear theory and coarsening of the phases is not observed possibly because of low surface energy difference between phases and 'locking-in' of the structure due to gelation.

3.3. Hydroxyl-terminated system

The reaction in the hydroxyl-terminated system was much slower compared to the vinyl-terminated system. These samples took 4–5 h to gel compared to 20 min in the vinyl-terminated system (Fig. 5). Initially, a ring pattern

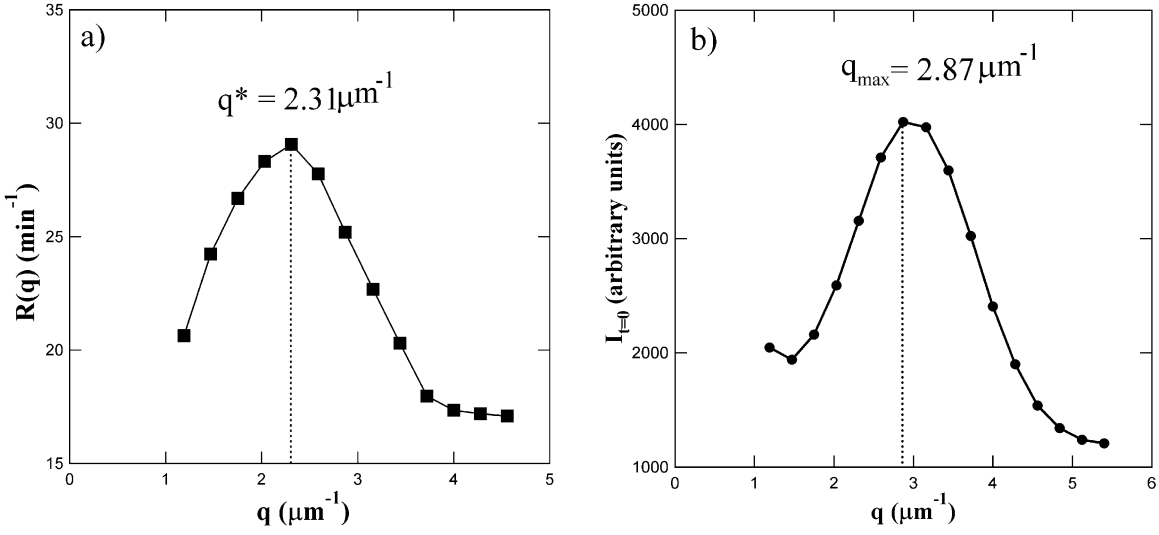

Fig. 10. (a) Rate of phase separation versus q; a maxima in growth rate occurs at wave-vector 2.31 μm^{-1}. (b) $I_{t=0}$ versus q, $I_{t=0}$ obtained from the intercepts in Fig. 9; maxima in $I_{t=0}$ occurs at 2.87 μm^{-1}.

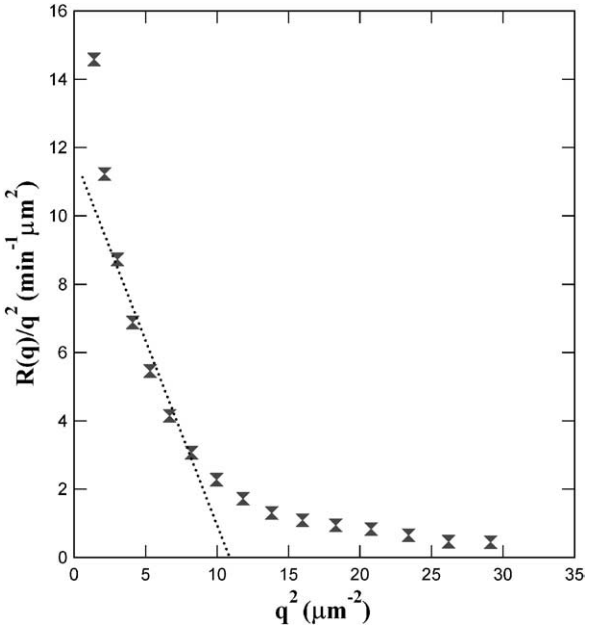

Fig. 11. Plot of $R(q)/q^2$ versus q^2 where the rate of phase-separation has been calculated form the slopes of Fig. 9. Dotted line follows Eq. (6). The x-intercept of the dotted line gives the value q^*.

observed in the hydroxyl-terminated system (Fig. 12 inset) was believed to be due to spinodal decomposition. But after inspection of optical micrographs (Fig. 12) it was found that low dispersion spherical domains formed, resulting in the ring pattern. The light scattering pattern, Fig. 12 (inset), displayed multiple concentric rings similar to the sphere function [41],

$$I(q) = \rho_0^2 v^2 \frac{9(\sin qR - qR\cos qR)^2}{(qR)^6} \tag{8}$$

where R is the sphere radius, q is previously defined, ρ^2 is the contrast ($\sim \Delta n^2$ for light scattering), and v is the volume of the spheres, assuming small difference in the refractive indices. The optical micrograph in Fig. 12 shows the morphology of the phases formed which are reminiscent of nucleation and growth. Fig. 13 is a log–log plot of scattered intensity versus wave-vector q for a sample with morphology as shown in Fig. 12. The data of Fig. 13 was fit using the maximum entropy method of Skilling and Bryan [42] that has been demonstrated to yield a good approximation of the particle size distribution for spherical particles [42–50].

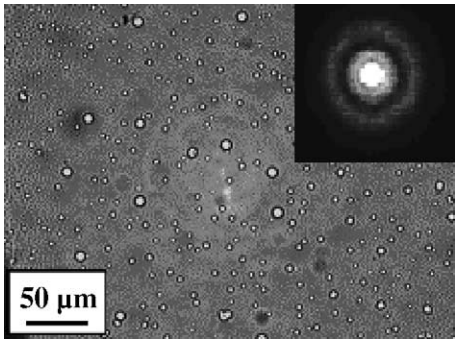

Fig. 12. Nucleation and growth observed in the hydroxyl-terminated system, inset shows the concentric ring pattern observed in light scattering from the specimen.

The code for the program is available on the web [43]. By fitting the scattered intensity using the maximum entropy method, the line in Fig. 13, the size distribution of the spherical domains was obtained as shown in Fig. 14.

Fig. 14 shows that the spherical domains display a bimodal volume distribution, consistent with the micrograph in Fig. 12. The distribution for the two modes are narrow, $\sigma \sim 1$ μm, indicating a narrow-time span for nucleation. The narrowly distributed domains are consistent with Fig. 5.

It is possible that the initial, rapid reaction to a low conversion in the condensation reaction leads to rapid nucleation on all existing heterogeneous nucleation sites in the sample. These early domains grow to the largest mode in Figs. 12 and 14, large domains of 9 ± 1 μm diameter. If all heterogeneous sites nucleate rapidly due to a rapidly rising branched fraction, a narrow distribution might result. The inhomogeneous spatial distribution of large domains might support heterogeneous nucleation as a source for the domains, Fig. 12, since heterogeneous nucleation might be expected to be inhomogeneously distributed in space.

Later, the slow production of highly branched species in the predominantly long-chain phase could lead to a second nucleation event in the gel network, with nucleation on regions of high crosslink density formed in the reaction. These domains are expected to be homogeneously-distributed spatially in the sample; small domains of Fig. 9. These late stage domains might be expected to be smaller since they nucleate later and since their growth occurs in a gel network. A somewhat broader distribution is also expected, 4 ± 2 μm as observed in Fig. 14 due to a relatively wider nucleation time-span. Nucleation might be terminated due to depletion of branched molecules in the long chain phase and due to network maturation at late stages. This discussion must remain speculative since the details of composition variations in such a reacting system are difficult to observe.

4. Conclusions

It has been shown in this work that it is possible to control the final morphology in a multi-component polymeric system through the rate of crosslinking reaction. Phase-separation can be induced by reaction in a bimodal network of short and long chains over a narrow set of conditions, including molecular weight of the precursors and their stoichiometry. Control of the reaction rate is the critical aspect for controlling phase-separation as not only thermodynamic, but kinetic parameters as well, control the phase-separation mechanism.

Increase in the molecular weights of the components due

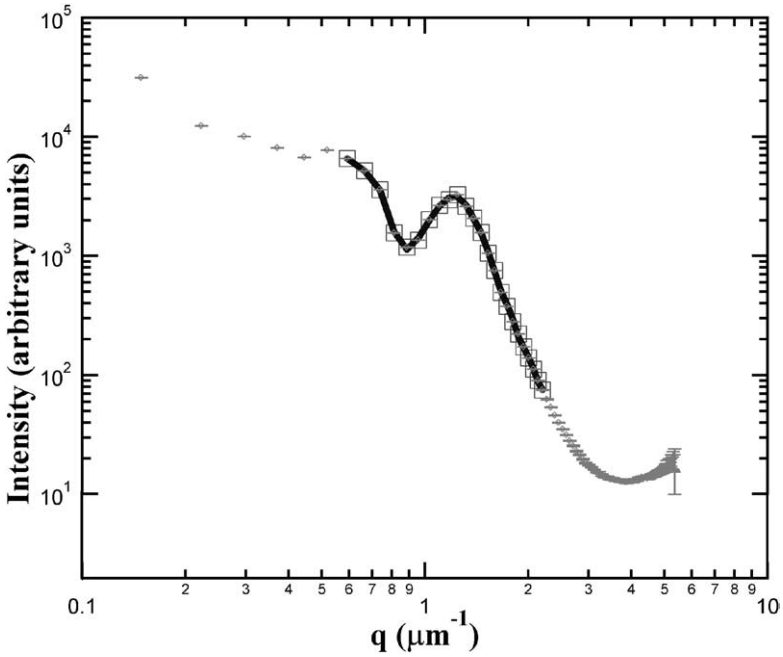

Fig. 13. Light scattering plot of log-scattered intensity versus log-q; line indicates a fit to the data using the maximum entropy method of Skilling and Bryan [42], as implemented by Beaucage et al. [44] and Jemian et al. [45] for polydisperse spheres, Fig. 12.

to crosslinking drives the proposed topological phase-separation. The phase-separated structure is 'locked-in' by network formation. Late-stage ripening is not observed possibly due to low surface energy difference in phase-separating topological systems and network formation. The kinetics of the early stages of spinodal decomposition, as described by the Cahn–Hilliard theory, are applicable to the rapid-reaction, vinyl-terminated system.

The reaction rate controls the effective 'quench-depth' of the system. In the vinyl-terminated system, where crosslinking takes place by an addition mechanism, phase-separation occurs by spinodal decomposition. The hydroxyl-terminated system follows the nucleation and growth mechanism of phase-separation. The reaction mechanism in the hydroxyl-terminated system is hydrolysis/condensation, which is slower as compared to the addition mechanism, and hence the quench depth is expected to be shallower.

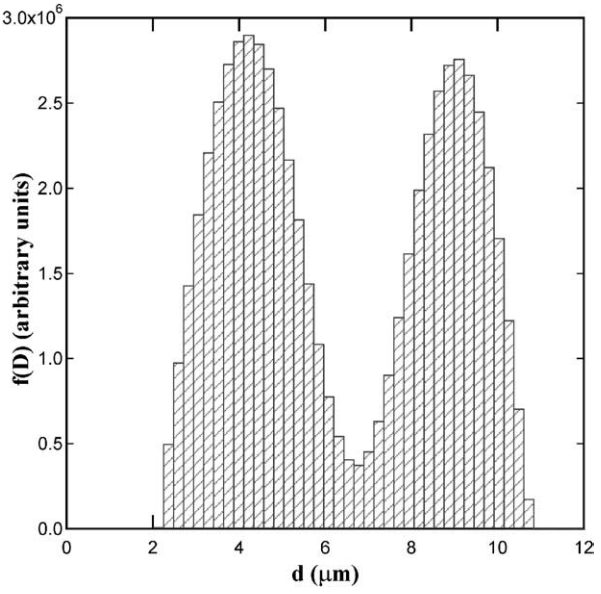

Fig. 14. Particle volume distribution function, $f(D)$, plotted against particle diameter, d, from fit of Fig. 13.

Phase separation in the hydroxyl-terminated system results in the formation of simultaneously nucleated, close-to-monodisperse spherical domains. The conversion rate associated with the condensation mechanism leads to two nucleation events with two characteristic sizes of domains associated with these nucleation events.

The role of branch topology in phase-separation of blends, as reported by Alamo et al., has been generalized and applied to our system. Both, vinyl as well as the hydroxyl-terminated systems, meet the critical requirement for initiation of phase-separation in terms of disparity in branch content of the two resulting phases. A lack of chemical difference between the phases by IR spectra, and from the reaction chemical makeup, supports topology as the source of immiscibility. It is shown that the refractive index difference associated with the crosslink density difference is sufficient to give rise to light scattering.

Acknowledgements

This work was inspired by previous efforts of Jim Mark and Brent Viers in studies of bimodal networks.

References

[1] Llorente MA, Andrady AL, Mark JE. J Polym Sci: Polym Phys Ed 1981;19:621–30.
[2] Mark JE. Adv Polym Sci 1982;44:1–26.
[3] Mark JE. Macromol Symp 2003;191:121–30.
[4] Briber RM, Bauer BJ. Macromolecules 1988;21:3296–303.
[5] Derouiche A, Bettachy A, Benhamou M, Daoud M. Macromolecules 1992;25:7188–91.
[6] Chen W, Li X, Dong T, Jiang M. Macromol Chem Phys 1998;199: 327–33.
[7] Inoue T. Prog Polym Sci 1995;20:119–53.
[8] Olabisi O, Robeson LM, Shaw MT. Polymer–polymer miscibility. New York: Academic Press; 1979.
[9] Viers B. PhD Dissertation, University of Cincinnati, 1998.
[10] Sharaf MA, Mark JE, Alshamsi AS. Polym J 1996;28:375–82.
[11] Cahn JW. J Chem Phys 1965;42:93.
[12] Cahn JW, Hillard JE. J Chem Phys 1968;28:258.
[13] Schulz M, Paul B. Phy Rev B 1998;58:11096–8.
[14] Kita R, Kaku T, Kubota K, Dobashi T. Phys Lett A 1999;259:302–7.
[15] deGennes PG. J Phys Lett 1979;40:69.
[16] deGennes PG. J Chem Phys 1980;72:4756.
[17] Wignall GD, Alamo RG, Londono JD, Mandelkern L, Stehling FC. Macromolecules 1996;29:5332–5.
[18] Roth LE, Valles EM, Villar MA. J Polym Sci, Polym Chem Ed 2003; 41:1099–106.
[19] Yuan Q, Mark JE. Macromol Chem Phys 1999;200:206–20.
[20] HyeonLee J, Guo L, Beaucage G, MacipBoulis MA, Yang AJM. J Polym Sci: Polym Phys Ed 1996;34:3073–80.
[21] Beaucage G. PhD Dissertation, University of Massachusetts, Amherst, 1991, p. 39, 121.
[22] Beaucage G, Stein RS, Hashimoto T, Hasegawa H. Macromolecules 1991;24:3443–8.
[23] Beaucage G, Stein RS. Macromolecules 1993;26:1609–16.
[24] Hashimoto T, Itakura M, Shimidzu N. J Chem Phys 1986;85:6773–86.
[25] Mirabella FM, Ford EA. J Polym Sci: Polym Phys Ed 1987;25: 777–90.
[26] Mirabella FM, Westphal SP, Fernando PL, Ford EA, Williams JG. J Polym Sci: Polym Phys Ed 1988;26:1995–2005.
[27] Nesarikar A, Crist B, Davidovich A. J Polym Sci: Polym Phys Ed 1994;32:641–6.
[28] Alamo RG, Graessley WW, Krishnamoorti R, Lohse DJ, Londono JD, Mandelkern L, et al. Macromolecules 1997;30:561–6.
[29] Odian G. Principles of polymerization. New York: Wiley; 1991.
[30] Bondi A. J Phys Chem 1964;68:441.
[31] Politzer P, Jin P, Murray SJ. Chem Phys 2002;117:8197–202.
[32] Atkins PW. Physical chemistry. San Francisco: W.H. Freeman Publishers; 1978. p. 756.
[33] Bohren CF, Huffman DR. Absorption and scattering of light by small particles. New York: Wiley; 1983.
[34] Cahn JW, Hilliard JE. J Chem Phys 1958;28:258.
[35] Cahn JW. J Chem Phys 1959;30:1121.
[36] Cahn JW, Hilliard JE. J Chem Phys 1959;31:688.
[37] Hashimoto T. Phase Transitions 1988;12:47–119.
[38] Gunton JD, San Miguel M, Sahni PS. In: Phase transitions and critical phenomena, vol. 8. Academic Press: New York; 1983. p. 269.
[39] Sugimoto T. Monodisperse particles. New York: Elsevier; 2000.
[40] Bansil R, Liao G, Falus P. Physica A 1996;231:346–58.
[41] Roe RJ. Methods of X-ray and neutron scattering in polymer science. New York: Oxford University Press; 2000. p. 160.
[42] Skilling J, Bryan RK. Monthly notices R. Astronom Soc 1984;211: 111–24.
[43] Ilavsky J. Particle Size Distribution from USAXS, A Manual for USAXS Analysis, UNICAT, Argonne Illinois, USA 2000, http://www.uni.aps.anl.gov/~ilavsky.
[44] Beaucage G, Kammler HK, Pratsinis SE. J App Cryst 2004;37: 523–35.
[45] Jemian PR, Weertman JR, Long GG, Spal RD. Acta Metall Mater 1991;39:2477–87.
[46] Boukari H, Long GG, Harris MT. J Colloid Interface Sci 2000;229: 129–39.
[47] Hansen S. Acta Cryst 1994;A50:547–50.
[48] Morrison JD, Corcoran JD, Lewis KE. J Appl Cryst 1992;25:504–13.
[49] Potton JA, Daniel GJ, Rainford BD. J Appl Cryst 1988;21:663–8.
[50] Tagliani A. Appl Math Comput 2000;112:333–43.